NASA-TM-111790

IN-02-TM
(C) WAIVED
008262

# AIAA-96-0230

# EFFECTS OF FIN LEADING EDGE SWEEP ON SHOCK-SHOCK INTERACTION AT MACH 6

Scott A. Berry and Robert J. Nowak
NASA Langley Research Center
Hampton, VA

**34th Aerospace Sciences Meeting & Exhibit**
January 15-18, 1996 / Reno, NV

For permission to copy or republish, contact the American Institute of Aeronautics and Astronautics
370 L'Enfant Promenade, S.W., Washington, D.C. 20024

# EFFECTS OF FIN LEADING EDGE SWEEP ON SHOCK-SHOCK INTERACTION AT MACH 6

*Scott A. Berry

and

**Robert J. Nowak
NASA Langley Research Center
Hampton, VA 23681

*The effects of fin leading edge sweep on peak heating rates due to shock-shock interaction have been experimentally examined in the Langley 20-Inch Mach 6 Tunnel. The shock interaction was produced by the intersection of a planar incident shock (16.8° shock angle relative to the freestream, generated by a 9° wedge) with the bow shock formed around a 0.5-inch diameter cylindrical leading edge fin. Heating distributions along the leading edge stagnation line have been obtained using densely spaced thin-film resistive-type sensors. Schlieren images were obtained to illustrate the very complex shock-shock interactions. The fin leading edge sweep angle was varied from 15-degrees swept back to 45-degrees swept forward for a freestream unit Reynolds number of $2x10^6$/ft. Two models were utilized during the study, one with 0.025-inch spacing between gage centers, and the other 0.015-inch spacing. Gage spatial resolution on the order of 0.015-in appeared to accurately capture the narrow spike in heating. Peak heating due to shock interaction was maximized when the fin was swept forward 15° and 25°, both promoting augmentations about 7 times the baseline value. The schlieren images for these cases revealed Type IV and Type III interactions, respectively.*

## Nomenclature

| | |
|---|---|
| $M_\infty$ | freestream Mach number |
| $Re_\infty$/ft | freestream unit Reynolds number (1/ft.) |
| Ch | non-dimensional Stanton number, $q/\rho_\infty u_\infty (h_{aw}-h_\infty)$ |
| $Ch_{ref}$ | reference Stanton number, measured for each run from undisturbed end of model |
| x | distance (in), measured from incident shock location |
| L | length of leading edge (4 in) |
| t | time (seconds) |
| $\lambda$ | fin sweep angle (degrees) |
| $\beta$ | incident shock angle (degrees) |
| $\delta$ | shock generator angle (degrees) |

## Introduction

Hypersonic flight vehicles are characterized by shock wave systems that, in general, lie close to the body and often generate highly complex two and three-dimensional shock-shock interaction regions with potentially high heating levels on surfaces near the interaction. This was clearly evident on the first manned hypersonic test vehicle, the X-15, where on a flight in which a ram-jet test article was attached to the ventral fin, structural damage to the engine pylon occurred as a result of shock impingement and the test article was lost in flight. Subsequent hypersonic flight vehicles, such as the Shuttle Orbiter, have, at some point in the design process, had to consider the possible ramifications of shock interactions on the aerothermal loads to the vehicle. The impact of shock interactions is especially important in the design of future hypersonic air-breathing cruise vehicles such as the (now canceled) National Aerospace Plane (NASP), see Figure 1, where leading edges of the scramjet inlet had to be designed to endure sustained and augmented heat loads.

Edney (1968) described the six basic interaction types, see Figure 2. Of the six, the Type IV interaction has generally been identified as the case with the highest heating augmentation, because a thin

* Research Engineer, Aerothermodynamics Branch.

** Research Engineer, Aerothermodynamics Branch, member AIAA.

supersonic jet is produced which can directly impinge on the surface. Heating level augmentations of over an order of magnitude higher than stagnation-point heating values have been reported in recent shock interaction studies, see for example Holden and Kolly (1995). A vast majority of the most recent studies, however, have dealt with the two-dimensional (2D) type interaction, typified by the so-called "shock-on-cowl" work initiated in support of the NASP program. The 2D interaction is generated by a planar bow or compression shock intersecting a shock formed around the engine cowl leading edge which is parallel to the plane of the incident shock. As a consequence of the NASP program, the 2D interaction has been extensively examined through a series of experimental and computational studies. Recent work by Hackett and Calleja (1995), Holden and Kolly (1995), Carlson and Wilmoth (1994), Prabhu (1994), and Vemaganti (1994) have provided, among other things, an increased understanding of the details of the interactions. Out of these studies came an appreciation for the instrumentation spatial density required to accurately define the heating distribution and narrow peak in regions of shock-shock interactions.

Contrary to the recent experimental and computational efforts conducted on the 2D type interaction, the three-dimensional (3D) "shock-on-fin" interaction has not been as extensively examined. The 3D interaction is typically generated by the intersection of a planar incident shock with a shock formed by a wing or strut leading edge (see Figure 1) which is perpendicular to the plane of the incident shock. Early 3D experiments by Bushnell (1965 and 1968), Heirs and Loubsky (1967), and Keyes and Haines (1972) were focused on the problem (of the time) of shock interaction on the swept back leading edges of wings, struts, and fins. (By convention, leading edges that are perpendicular to the freestream flow are said to have no sweep, while leading edges that are swept away from the flow are referred to as swept back.) These studies did not address the problem of forward sweep where the potential is strongest for a Type IV interaction to generate a supersonic jet which impinges normal to the surface. The heating distribution associated with this "strong" Type IV would be such that instrumentation resolution would be critical for accurately measuring the strong and narrow peak. For current applications, such as the internal surfaces of scramjet engines, swept forward leading edges (relative to the incident shock) and strong Type IV interactions are possible. Thus, for conditions where the Type IV interaction heating would be maximized, an experimental dataset was not available for comparison to recent 3D computational efforts by Singh, Kumar, and Tiwari (1990 and 1993).

The current study systematically examines the effect of fin leading edge sweep on the shock-shock interaction process at Mach 6. Two highly instrumented cylindrical leading edge fins, 0.5-inch in diameter, were subjected to a planar shock generated with a two-dimensional sharp leading edge wedge. The models were capable of arbitrary fin sweep angles between ±45° (backward/forward). Detailed heating distributions along the stagnation line of the cylinder were measured with thin film resistance gages. The first model, which is considered the baseline model, was fabricated using conventional mechanical deposition techniques and had a minimum center-to-center gage spacing of 0.025 inch. The second model was fabricated using less-conventional techniques and had a minimum center-to-center gage spacing of 0.015 inch. (The second model, which was considered experimental in nature, was tested for only a limited number of runs to compare with the baseline model.) These measurements were complemented with high quality schlieren photography. Over sixty wind tunnel runs have been conducted over a range of fin sweep angles. The purpose of this paper is to present these initial results which detail the effect of fin sweep angle on shock interaction heating for the fixed conditions of 0.5-inch diameter leading edge, 16.8° incident shock angle, freestream Mach number of 6, and freestream unit Reynolds number of $2 \times 10^6$/ft. Also presented are qualitative results in the form of schlieren images obtained over a range of Reynolds numbers for 0° and 20° swept forward fin sweep angles. The current experimental results provide a better understanding of the complex nature of 3D interactions and are applicable for future 3D shock interaction code calibration efforts.

## Experimental Methods

### Facility

The experiment was conducted in the 20-Inch Mach 6 Tunnel at the NASA Langley Research Center. A detailed description of this facility, along with performance characteristics, is provided by Miller (1990). It is a hypersonic blowdown facility which uses heated, dried, and filtered air as the test gas. Typical operating conditions for the tunnel are stagnation pressures ranging from 30 to 500 psia, stagnation temperatures from 760° to 1000°R, and

freestream unit Reynolds numbers from 0.5 to $9x10^6$/ft. A two-dimensional, contoured nozzle is used to provide nominal freestream Mach numbers from 5.8 to 6.1. The test section is 20.5 by 20 inches; the nozzle throat is 0.399 by 20.5 inch. A bottom-mounted model injection system can insert models from a sheltered position to the tunnel centerline in less than 0.5 seconds. Run times up to 15 minutes are possible with this facility, although for the current heat transfer tests run times were only a few seconds. As discussed by Micol (1995), the tunnel has 256 channels of signal conditioning for the thin-film instrumentation. These channels are interfaced to a 16-bit, analog-to-digital data acquisition system which typically interrogates each channel at a rate of 50 samples per second.

For a majority of the current study, both heating measurements and schlieren images were acquired on the 0.025 inch spacing thin-film baseline model at a freestream unit Reynolds number of $2x10^6$/ft. A few of the fin sweep cases were repeated with the 0.015 inch spacing model. A limited number of schlieren only runs were acquired over a range of freestream unit Reynolds number of $0.5x10^6$/ft to $8x10^6$/ft. Table 1 presents the nominal flow conditions for these cases.

Models

The experimental set-up (sketched in Figure 3) consists primarily of a sharp leading edge, two-dimensional, flat plate shock generator, and a cylindrical leading edge fin that is instrumented with densely-spaced thin-film gages. The uninstrumented stainless-steel shock generator is 6 inches wide by 17 inches long and was set at a shock generator angle ($\delta$) of 9° relative to the freestream flow, which produces an incident shock angle ($\beta$) of 16.8° relative to the freestream flow. The sweep-adjustable fin was held above the shock generator in order to place the fin root out of the boundary layer on the shock generator plate. This was done to isolate the shock interaction process from the shock/boundary-layer interaction process at the base of the fin. The fin leading edge consisted of a 4 inch long instrumented Macor cylinder which was 0.5-inch in diameter. (Macor is a machinable glass ceramic that is a trademark of Corning Glass Works). The fin can be adjusted for fin sweep angles ($\lambda$) from ±45° with repeatable accuracy of better than 1°. As can be seen in the sketch, a removable sweep adjustment indicator was provided to assist in the accurate setting of the fin sweep angle prior to a run. The thin-film gages were spaced along the leading edge stagnation line (or more accurately the attachment line when the fin is at a non-zero fin sweep). A photograph of the model installed in the 20-Inch Mach 6 Tunnel is shown in Figure 4.

Instrumentation

Previous shock interaction studies have revealed the importance of instrumentation resolution in order to accurately capture the heating peaks associated with the interactions. Experimental work such as Wieting (1987) or Holden and Kolly (1995) on the 2D case utilized models which had gage centers spaced circumferentially about 0.8° apart in the interaction region. The CFD work of Prabhu (1994) indicated that for a Type IV interaction the width of the peak value of heating is on the order of 1.0°. Assuming that 3 points are required to define the peak, a gage spacing on the order of 0.5° is required for the 2D case. Thus the actual gage resolution of these 2D studies nearly match the instrumentation requirements predicted by computational methods. To date (as far as the authors are aware), 3D simulations for the Type IV case, where the jet impinges normal to the surface, have not been published (computations by Singh, et. al. (1993) were for a lower heating "glancing" Type IV case). Guidance on the spatial resolution for the 3D case is not available. Thus, for the present study, emphasis was placed on the development of thin-film instrumented models which provided an improvement in gage resolution over previous 3D shock interaction studies.

Standard mechanical deposition techniques (such as vapor-deposition or sputtering) have been used at LaRC to produce high-quality thin-film resistive type gages in the past (see Miller, 1981). However, the best resolution that was obtainable using these techniques on a cylindrical Macor rod was 0.025-inch spacing between gage centers. The gages for this baseline model were mechanically deposited using vapor deposition. The limiting factor for fabrication of this model was the width of the sensor leads, or, more precisely, the ability of the fabrication technique to accurately maintain the clearance between the leads on a cylindrical surface. The main difficulty with using standard mechanical deposition techniques is that line-of-sight apparatuses are generally used during the fabrication process, which makes it difficult to place high-quality, tightly-packed gages and leads onto curved surfaces.

While standard techniques were used to provide a baseline model, new approaches were also examined to improve the leading edge spatial resolution. One of the more promising approaches involved the use of

a thin polyimide film as a transfer medium to place high-quality gages down on a curved surface. The thin-film gages were etched onto a flat polyimide film and the film was later wrapped and bonded to the cylindrical rod. Using this technique the thin-film gage resolution was improved to 0.015-inch spacing between gages. (With this technique it is possible to deposit sensors whose spacing is 0.005". On this scale, the difficulty is finding the space to route the leads away from the sensors.) The polyimide film that was chosen during the development process was a 50 μm (0.002-inch) thick Type S Upilex film because its excellent surface quality allowed for high quality gages. (Upilex is a registered trademark of Ube Industries, Ltd.)

Another technique which was considered was the use of the thin-film painting technique which is described in some detail by Vidal (1956) and Ligrani, et. al. (1982). A cylindrical Macor rod with high spatial gage resolution of 0.010" was fabricated, but unfortunately damaged during the annealing process. Although subsequently repaired, this model was not available for the present study. (This technique has the disadvantage of being very labor intensive, requiring many hours to hand paint extremely fine gages and tightly packed leads, and to solder the many leads which are in close proximity to each other.)

Thus two instrumented models were available during this study, the baseline standard Macor model which had a total of 80 gages with a resolution of 0.025" over a 1 inch section near where the interaction was to occur, and the new Upilex model which had a total of 108 gages with a resolution of 0.015". On both models the spacing requirements were relaxed for the remainder of the 4-inch leading edge with regions where the gage spacing was 0.050" and 0.100". Photographs of the instrumented cylinders used in this study are presented in Figure 5. The Macor model has 0.002" x 0.100" palladium sensors that are connected to a combination of gold and silver leads. The Upilex model has 0.002" x 0.100" nickel sensors that are connected to a combination of nickel and copper leads.

To investigate the shock interaction process in more detail, a single-pass, magnifying lens schlieren system was set-up to zoom-in and capture a 2 inch diameter area centered around the point of shock-shock interaction (see Figure 3). A xenon light source was used providing a flash duration of approximately 1-2 μsec. The images were recorded on 4 by 5 inch black-and-white film, and 30 frame/sec. video. The model was front-lighted to illuminate the gages on the picture for a scale reference.

Data Reduction and Uncertainty

Calibrations, in a uniform temperature oil bath, over a temperature range of 75° to 425°F were performed on both models. The resistivity of palladium is reported to be essentially linear over this temperature range and this was confirmed by the calibrations. However, for the Upilex model, nickel was chosen as the sensor material (mainly due to its high temperature sensitivity) which has a more non-linear response to changes in temperature. Thus, a second-order curve fit was used for the Upilex model to convert the millivolt output of the gages to temperature.

Data reduction was performed using a newly-developed code written by Hollis (1995). Both an analytical, based on the method of Cook and Felderman (1966), and a numerical (finite-volume) heat transfer scheme are incorporated into this code. The analytical solution is developed on one-dimensional, semi-infinite solid heat conduction theory based on constant thermal properties of the substrate. When using this option the inferred heating rates are empirically corrected for the effects of variable thermal properties. Hollis and Perkins (1995) compares this analytical technique to others, including the finite volume technique, and shows excellent agreement (1-2% error). Thus, the Macor model was analyzed using the analytical technique. The finite volume technique directly accounts for the variable substrate thermal properties and removes the restriction of a semi-infinite substrate (thus allowing for a multiple layer analysis). This was an important consideration for the Upilex model, as, for the test times associated with conventional hypersonic facilities, the thermal penetration depth of the heat pulse will exceed the thickness of the polyimide film and invalidate the semi-infinite assumption. Thus, for the Upilex model the heat transfer was computed using the finite volume technique, with 5 points in the Upilex layer and 244 points in the Macor sublayer. Recent updates to the thermal properties of both Macor and Upilex have been included in the code and are discussed in Hollis (1995). The current analysis of the Upilex model data has been conducted with the assumption that the approximately 0.001-inch bondline is thermally invisible. Reliable thermal property information for the adhesive that was used (Duralco #4525 high temperature epoxy) is not currently available. Thermal property analysis of the bonding material, as well as further analysis of the polyimide film, is on-going.

The individual thin-film resistance type sensors provided temperature-time histories that were

integrated to compute the heating rate and normalized to provide Stanton numbers, Ch. Primary contributions to the uncertainty in the heat transfer results include the uncertainties associated with the thermal properties of the substrate material (including the neglected bond layer) and possible violations to the one-dimensional assumption due to the strong heating gradient in the vicinity of the interaction providing mechanisms for lateral conduction. To minimize the effect of the error associated with the thermal properties on the comparisons between the two models, the Stanton number calculated for each gage was normalized by the calculated Stanton number for an average of gages that were on the undisturbed portion of the cylinder during each run. A comparison, between the two models, of the normalized Stanton number histories for the peak heating gages for the case of shock impingement with fin sweep of 0° is shown in Figure 6. In the figure, a time of t=0 seconds corresponds to the start of injection and at t=2 seconds the model has stopped at tunnel centerline. The Stanton number remains constant with time once the model reaches centerline and, consequently, the distributions shown in the following section are based on time averaged data for a 1 second interval starting at t=2 seconds. Smaller averaging windows were examined with minimal effect on the overall distribution or peak.

## Results and Discussion

Heat transfer measurements and schlieren images were obtained for a range of fin sweep angles that varied between +15° (swept back) and -45° (swept forward) for a freestream unit Reynolds number of $2x10^6$/ft. The results presented in Figures 7 through 15 are for a roughly 5° increment (a finer increment in fin sweep angles was obtained and these results will be included in the summary peak heating plot in Figure 16). The images were used to identify the location of the extrapolated position of the incident shock as shown in the labeled schlieren image that was included within the sketch of Figure 3. The width of the planar incident shock is wider than the breadth of the fin bow shock. Therefore, the incident shock appears in the image to continue through the initial triple point, thereby locating the exact gage number of the x=0 location. By transferring x/L to the incident shock location, the heating distributions collapse on top of each other even though the actual location of the impingement may differ run to run. As will be shown in the subsequent heat transfer distributions, excellent agreement was found in the overall trends between different runs in which both the location of the model, as well as the model type, was varied. It should be noted that in some of the close-up schlieren images, unusually wide incident shocks occur. This appears to be attributable to a non-planar shock condition set-up by defects to the leading edge corners of the shock generator which occurred due to handling.

### Fin Sweep of 15°

The flow-visualization and heating results for the case where the fin leading edge was swept back 15° are presented in Figure 7. The schlieren image (fig. 7a) reveals an interaction (perhaps a Type V) that produces a very small transmitted shock that remains close to the triple point. The resulting shear layer is turned up at an angle such that reattachment occurs quite some distance above the extrapolated position of the incident shock. This is consistent with the heating results (fig 7b) which reveal that, in general, the overall heating levels are quite low (at most 1.5 times the undisturbed value) and that reattachment occurs midway up on the leading edge (at $x/L \approx 0.2$).

### Fin Sweep of 0°

Figure 8 shows the results for the case where the fin sweep angle is 0° (the leading edge is perpendicular to the freestream). The schlieren results (fig 8a) reveal that a "glancing Type IV" interaction has been set up where the supersonic jet bends up and away from the fin leading edge. The reattachment region appears to be closer to the extrapolated position of the incident shock (i.e. the $x/L = 0$ position) as compared to the previous example. The heating results in figure 8b confirm this and also show that the heating augmentation due to the reattaching flow is increasing

### Fin Sweep of -10°

The results for the 10° swept forward case are presented in Figure 9. The schlieren photo (fig 9a) reveals that the transmitted shock length has increased slightly and that the shear layer remains below the $x/L = 0$ location, resulting in a more classic Type IV interaction. There appears to be a slight upward inclination of the terminating jet, however. The heating results (fig 9b) reveal that indeed a strong and narrow peak has emerged with a peak value of heating a little over 4 times the baseline value.

Fin Sweep of -15°

Figure 10 presents the results for the case where the fin leading edge is swept forward 15°. The fin is now nearly perpendicular to the incident shock, as seen in Figure 10a The transmitted shock length has increased and the Type IV interaction now terminates directly into the fin leading edge just below the incident shock location. The heating results, figure 10b, reveal a strong and narrow peak augmentation with secondary peaks on either side. The peak heating value is on the order of 7 times the baseline value. Although not visible in Figure 10a, the gage leads can be traced forward to show that, for the 0.015-inch spacing model, the supersonic jet width appears to be on the order of the distance between three of the gages.

Fin Sweep of -20°

The results for the 20° swept forward case are presented in Figure 11. The schlieren image shows that the transmitted shock length has become quite long, such that the shear layer has begun to directly impinge on the fin leading edge without further processing by the supersonic jet shock system. The heating results show a slight reduction in the overall peak heating value as well as a slight broadening of the high heating zone

Fin Sweep of -25°

The results for the 25° swept forward case are presented in Figure 12. The schlieren results, shown in fig 12a, reveal that the interaction is becoming more like a Type III interaction, where the shear layer emerging from the first triple point dominates the surface impingement process. This is verified by the heating results (fig 12b), as the peak heating location corresponds to the thin-film gage directly in line with the shear layer in the schlieren photograph for all four runs. The overall peak heating level is again around 7 times the baseline value, and the peak width has broadened significantly.

Fin Sweep of -30°

Figure 13 presents the results for the case where the fin leading edge is swept forward 30°. The interaction (see fig 13a) is beginning to resemble a Type II interaction, although the shear layer emanating from the initial triple point still appears to dominate the surface impingement process. The heating results confirm this (see fig 13b) as a strong peak (with overall peak heating level of 5 times the baseline value) coincides with the thin-film gages directly under the shear layer impingement. The width of the main peak is quite broad and a minor secondary peak is evident which may correspond to the reattachment of the shear layer emanating from the secondary triple point.

Fin Sweep of -35°

The results for the 35° swept forward case are presented in Figure 14. The schlieren image reveals a Type II interaction that appears to support a complex merging of the shear layers associated with the two different triple points. The heating results reveal a continued breakdown of the primary peak as well as strengthening of the secondary peak. The overall peak heating level has dropped down to just over 3 times the baseline value.

Fin Sweep of -45°

Figure 15 presents the results for the case where the fin leading edge is swept forward 45°. A Type I interaction has emerged (see fig 15a), which involves a complex pattern of crossing shock and shear layers. The heating results (fig 15b) show that the peak heating location corresponds to the initial impingement point just below the extrapolated incident shock location. The overall peak heating level is just over 3 times the baseline value.

Peak Heating due to Fin Sweep

Figure 16 presents the results of the peak heating values as function of fin leading edge sweep angle. The data is fitted with a smoothed curve to provide an indication of the trends with fin sweep angle with separate curves for the Macor and Upilex models. A double humped trend is evident, with peaks at both the 15° and 25° swept forward cases. The $\lambda$=-15° case corresponds to a Type IV interaction while the $\lambda$=-25° case corresponds to a Type III. The Upilex model shows approximately a 15-20% overall increase in peak heating level, which is believed to be partially attributable to the increased spatial resolution of the Upilex model.

Reynolds Number Effects

Although the heat transfer results were for a single freestream unit Reynolds number, a limited number of schlieren only runs were obtained over the Reynolds number range of 0.5 to 8.0 million per foot. Figure 17 presents the results for this Reynolds number range for the case where the fin is swept 0°. Figure 18 presents the results for this same range for the case where the fin is swept forward 20°. In both cases, the shear layer or jet emanating from the triple point appears to break up and become

more diffuse as the Reynolds number increases (perhaps as an indicator of unsteadiness associated with transition and turbulence). Also noteworthy are the large scale vortices which form along the surface for the $\lambda$=-20° case which is particularly evident in Figures 18b and 18d.

Small Fin Sweep Increments

An example of the extreme sensitivity of shock interaction type to fin sweep is presented in Figure 19 where a 1° sweep change produced a marked difference in shock pattern. The image corresponding to a fin sweep of -38° is an example of a Type II interaction, while the image corresponding to a fin sweep of -39° is an example of a Type I interaction. Both of these cases were acquired at a freestream unit Reynolds number of $2 \times 10^6$/ft.

## Concluding Remarks

A study to examine the effect of fin leading edge sweep angle on the shock interaction process has been performed in the NASA Langley 20 Inch Mach 6 Tunnel. The shock interaction was produced by the intersection of a planar incident shock and a bow shock formed around a 0.5-inch diameter cylindrical leading edge fin. The fin sweep angle was varied from 15° swept back to 45° swept forward. Heating distributions along the stagnation line of the swept fins subjected to a 16.8° (relative to the freestream flow) incident shock were obtained. These distributions were complemented with schlieren photography to illustrate the complex interactions. A finer fin sweep angle increment was used, as compared to previous 3D studies, with emphasis placed on the forward swept cases which potentially produces the highest peak heating augmentations. Also, a significant improvement in the spatial density of the thin-film gages, critical to the accurate measurement of peak heating values, was accomplished for the present study.

The results indicate that for 3D shock interactions, heating augmentations drastically increase when the leading edge of the fin is swept forward towards the incident shock. Peak heating was maximized when the fin was at $\lambda$=-15° and $\lambda$=-25°. A Type IV interaction occurred when the fin sweep angle was nearly perpendicular to the incident shock ($\lambda$=-15°). This produced a peak heating augmentation of 7 times the baseline value. An equally high peak heating value was measured at a fin sweep angle which produced a Type III interaction ($\lambda$=-25°). Using the leads as a scale reference in the schlieren images, at least 3 gages were within the width of the jet associated with the Type IV cases, which is an indication that the gage resolution was adequate.

## Acknowledgments

Without the assistance of the following, this paper would not have been possible: Ed Self, Jim Bartlett, Steve Parrish, Greg Draughon, and Johnny Mau for instrumentation support; Dave Rhodes and Steve Jones for schlieren expertise; Rhonda Manis, Grace Gleason, and Johnny Ellis for tunnel support; Bert Senter and Sheila Wright for DAS assistance; Tom Horvath, Brian Hollis, and Charlie Hackett for design and/or analysis support and; Richard Wheless and Nan Judge for documentation assistance. The authors gratefully acknowledge their contribution.

## References

Bushnell, Dennis M. (1965): "Interference Heating on a Swept Cylinder in Region of intersection With a Wedge at Mach Number 8," NASA TN D-3094, December 1965.

Bushnell, Dennis M. (1968): "Effects of Shock Impingement and Other Factors on Leading-Edge Heat Transfer," NASA TN D-4543, April 1968.

Carlson, Ann B. and Wilmoth, Richard. G. (1994): "Monte Carlo Simulation of a Near-Continuum Shock-Shock Interaction Problem." Journal of Spacecraft and Rockets, Vol. 31, No. 1, January-February 1994.

Cook, W. J. and Felderman, E. J. (1966): "Reduction of Data from Thin-Film Heat-Transfer Gages: A Concise Numerical Technique," AIAA J. Vol. 4, No. 3, March 1966.

Edney, B. (1968): "Anomalous Heat Transfer and Pressure Distributions on Blunt Bodies at Hypersonic Speeds in the Presence of an Impinging Shock," The Aeronautical Research Institute of Sweden, Report 115, 1968.

Hackett, C. M.; and Calleja, J. (1995): "Exploratory Study of Heating Due to a Hypersonic, High-Enthalpy Shock/Shock Interaction," Presented at the 26th AIAA Fluid Dynamics Conference, June 19-22, 1995, AIAA 95-2216.

Heirs, R. S. and Loubsky, W. J. (1967): "Effects of Shock-Wave Impingement on the Heat Transfer on a Cylindrical Leading Edge," NASA TN D-8859, February 1967.

Holden, M. and Kolly, J. (1995): "Measurements of Heating in Regions of Shock/Shock Interaction in Hypersonic Flow," AIAA 95-0640, January 1995.(Sponsored by NASA LaRC Grant NAG-1-1339).

Hollis, B. R. (1995): "User's Manual for the One Dimensional Hypersonic Experimental Aero-Thermodynamic (1DHEAT) Data Reduction Code," NASA Contractor Report 4691, August 1995.

Hollis, B. R. and Perkins, J. N. (1995): "Hypervelocity Aeroheating Measurements in Wake of Mars Mission Entry Vehicle," AIAA Paper 95-2314, 1995.

Keyes, J. W. and Haines, F.D. (1973): "Analytical and Experimental Studies of Shock Interference Heating in Hypersonic Flow," NASA Report TN D-7139, May 1973.

Ligrani, P. M.; Camci, C.; and Grady, M. S. (1982): "Thin Film Heat Transfer Gage Construction and Measurement Details," von Karmin Institute for Fluid Dynamics TM 33, November 1982.

Micol, J. R. (1995): "Hypersonic Aerodynamic/ Aerothermodynamic Testing Capabilities at Langley Research Center: Aerothermodynamic Facilities Complex," AIAA 95-2107, June, 1995.

Miller, C. G. (1981): " Comparison of Thin-Film Resistance Heat-Transfer Gages with Thin-Skin Transient Calorimeter Gages in Conventional Hypersonic Wind Tunnels," NASA TM-83197, December 1981.

Miller, C. G. (1990): "Langley Hypersonic Aerodynamic/Aerothermodynamic Testing Capabilities - Present and Future," AIAA 90-1376, June 1990.

Prabhu, Ramadas K. (1994): "An Implementation of a Chemical and Thermal Nonequilibrium Flow Solver on Unstructured Meshes and Application to Blunt Bodies," NASA LaRC Contractor Report 194967, Lockheed Engineering and Sciences Company, Hampton, Virginia 23666, August 1994.

Singh, D. J.; Kumar, A.; and Tiwari, S. N. (1993): "Numerical Simulation of Three-Dimensional Shock-Shock Interactions on a Blunt Body," *Comp. Fluid Dyn.*, 1993, Vol. 1, pp 177-196.

Singh, D. J.; Kumar, A.; and Tiwari, S. N. (1990): "Three-Dimensional Shock-Shock Interactions on The Scramjet Inlet," Presented at the 28th Aerospace Sciences Meeting, Reno Nevada, January 8-11, 1990, AIAA Paper No. 90-0529.

Vemaganti, Gururaja R. (1994): "Laminar and Turbulent Flow Computations of Type IV Shock-Shock Interference Aerothermal Loads Using Unstructured Grids," NASA LaRC Contractor Report 195008, Lockheed Engineering and Sciences Company, Hampton, Virginia 23666, October 1994.

Vidal R. J. (1956): "Model Instrumentation Techniques for Heat Transfer and Force Measurements in a Hypersonic Shock Tunnel," Cornell Aeronautical Laboratory Report AD-917-A-1, Buffalo, NY, February 1956.

Wieting, Allan R. (1987): "Experimental Study of Shock Wave Interference Heating on a Cylindrical Leading Edge," NASA TM 100484, May 1987.

| $Re_\infty$/ft | $P_{t1}$ (psi) | $T_{t1}$ (°R) | $\rho_\infty$ (slug/ft$^3$) | $T_\infty$ (°R) | $u_\infty$ (ft/sec) | $M_\infty$ |
|---|---|---|---|---|---|---|
| 0.5 | 30 | 869 | $0.17 \times 10^{-4}$ | 111 | 3019 | 5.84 |
| 2.0 | 125 | 910 | $0.63 \times 10^{-4}$ | 113 | 3093 | 5.93 |
| 4.0 | 260 | 935 | $1.23 \times 10^{-4}$ | 114 | 3139 | 5.98 |
| 8.0 | 475 | 935 | $2.18 \times 10^{-4}$ | 113 | 3142 | 6.02 |

Table 1: Nominal flow conditions for 20-Inch Mach 6 Tunnel.

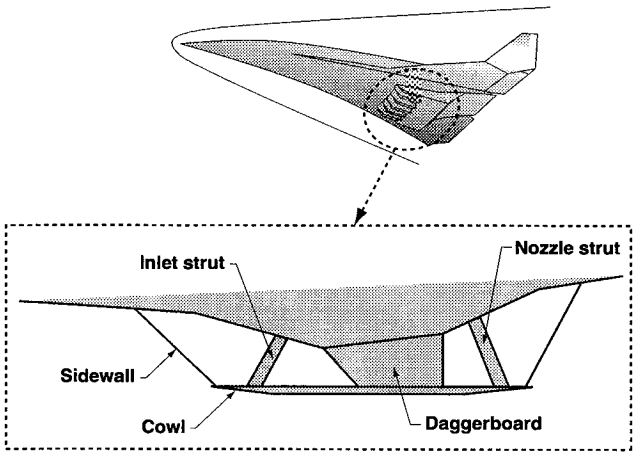


Figure 1: Shock interaction regions for a hypersonic airbreathing cruise vehicle.

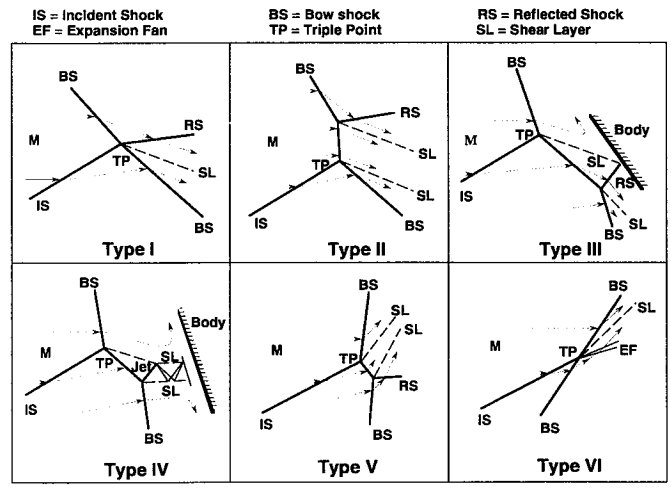


Figure 2: Shock interaction types as classified by Edney (1968).

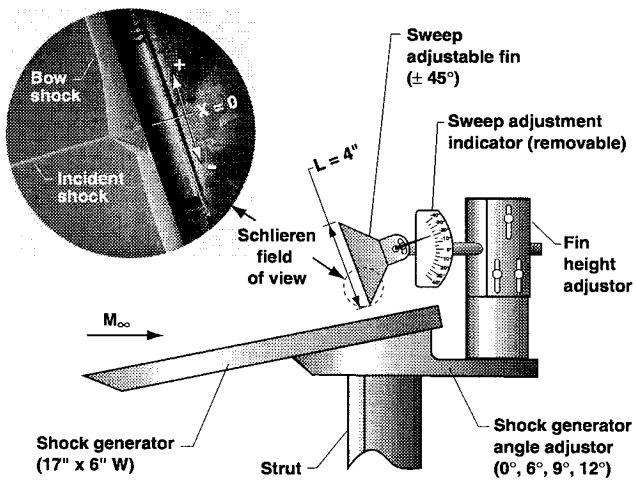


Figure 3: Sketch of experimental set-up.

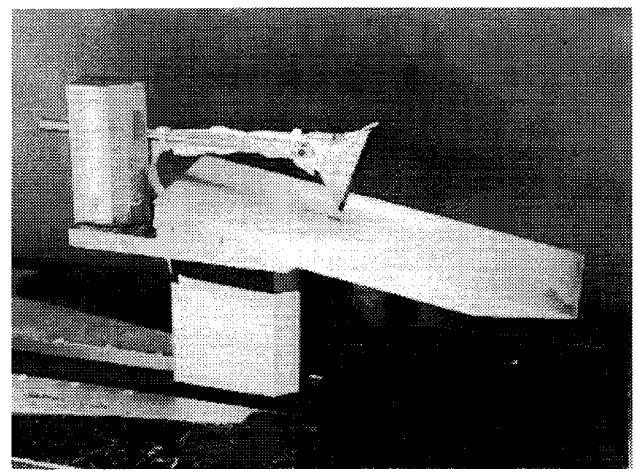

Figure 4: Photograph of model installed in LaRC 20" Mach 6 Tunnel.

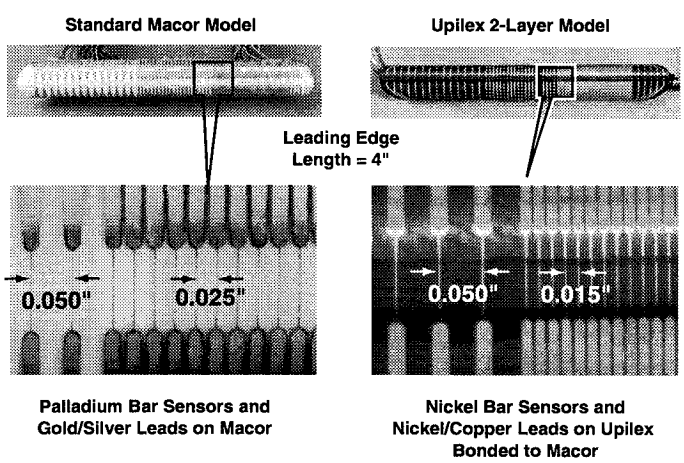


Figure 5: Details of thin-film instrumentation.

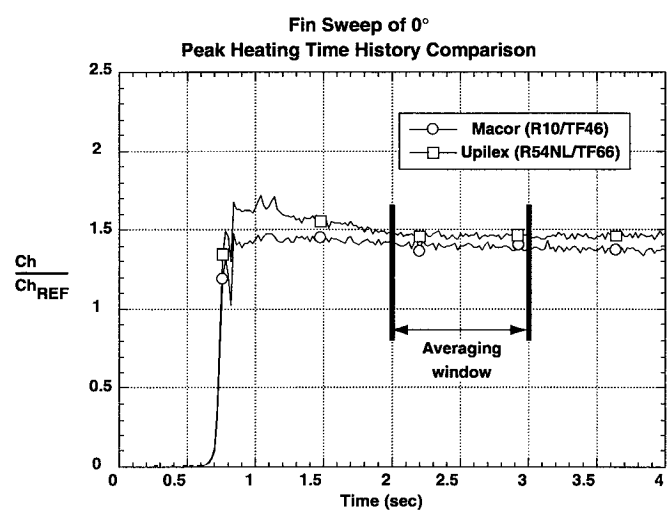


Figure 6: Comparison of normalized heating time histories for peak heating gages between both models for shock on fin case of 0° sweep.

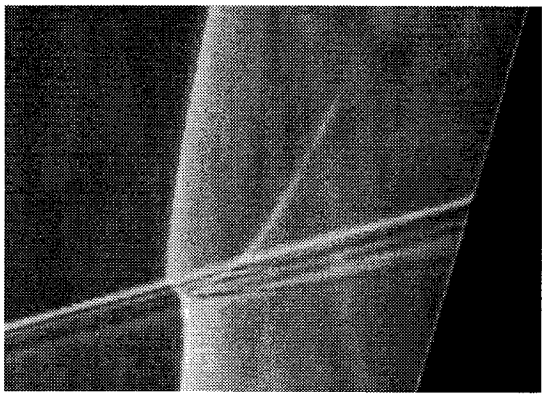

(a) Schlieren image.

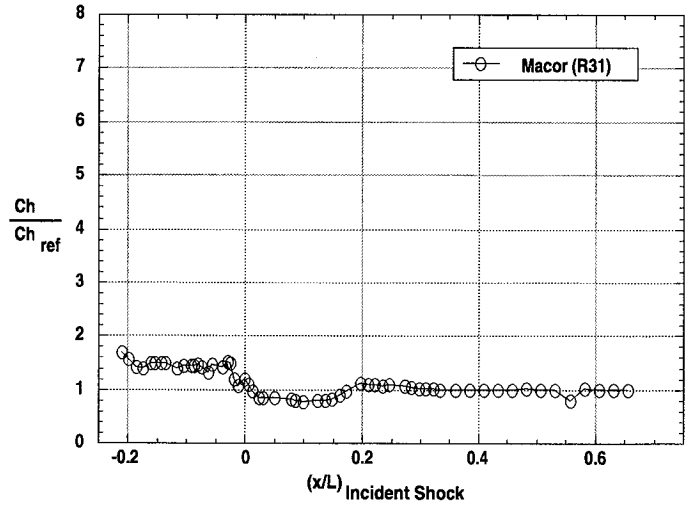


(b) Heating distribution.

Figure 7: Results for $\lambda = 15°$.

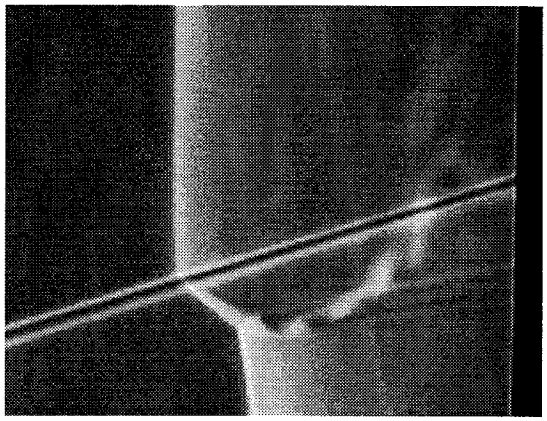

(a) Schlieren image.

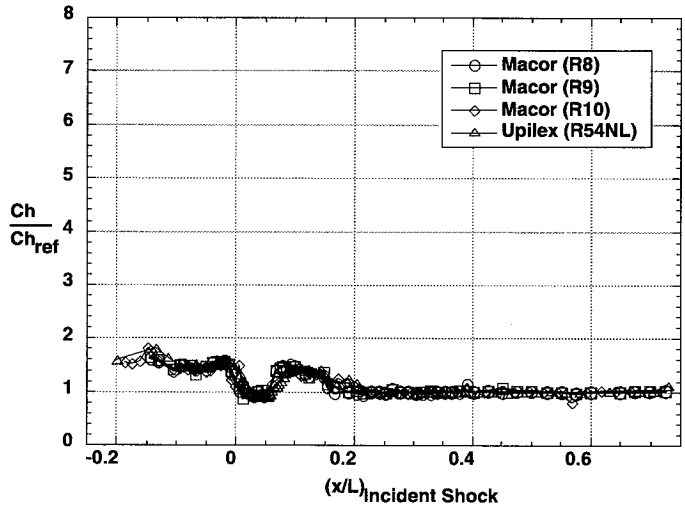


(b) Heating distribution.

Figure 8: Results for $\lambda = 0°$.

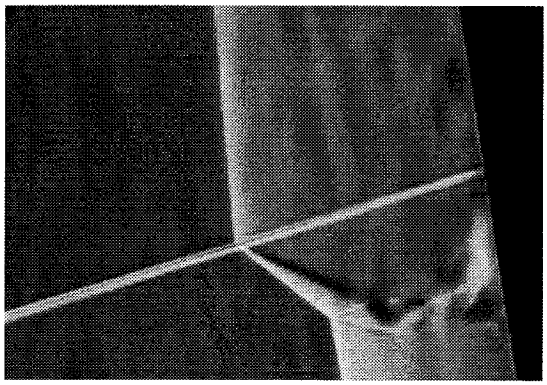

(a) Schlieren image.

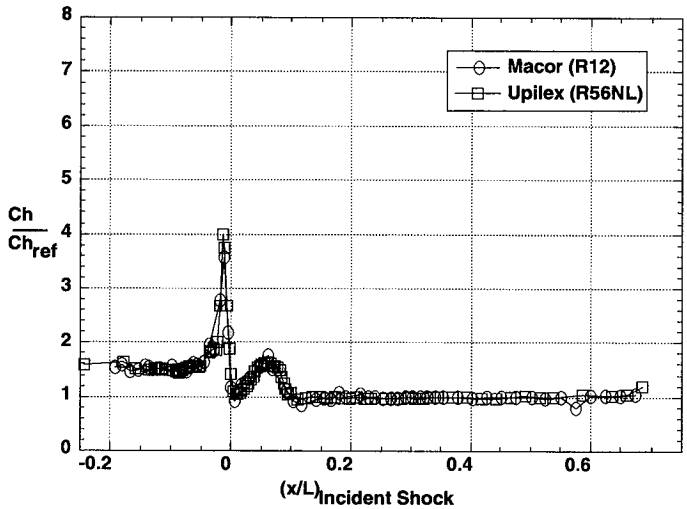


(b) Heating distribution.

Figure 9: Results for $\lambda = -10°$.

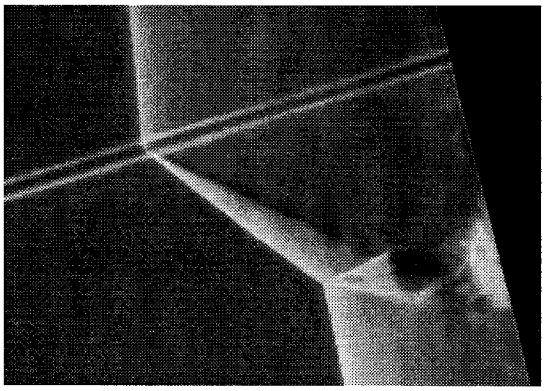

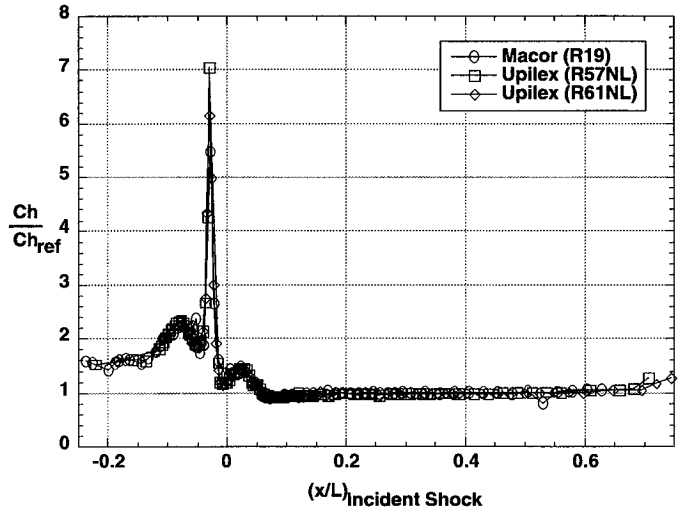


(a) Schlieren image. (b) Heating distribution.

Figure 10: Results for $\lambda = -15°$.

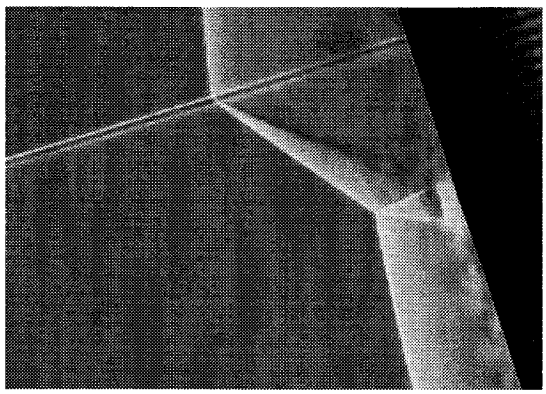

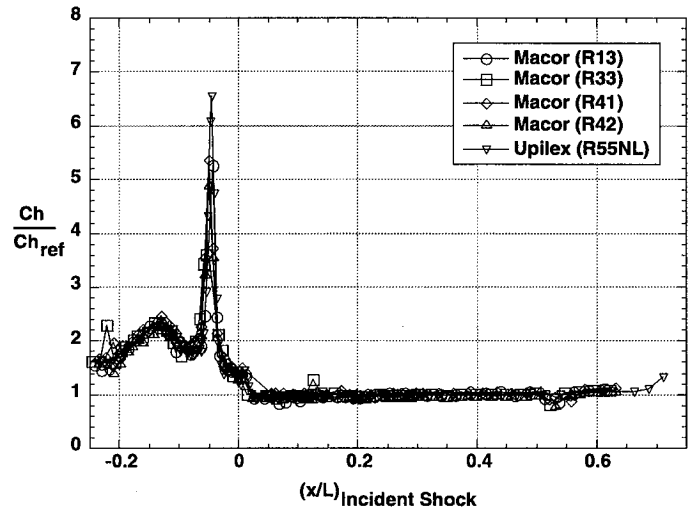


(a) Schlieren image. (b) Heating distribution.

Figure 11: Results for $\lambda = -20°$.

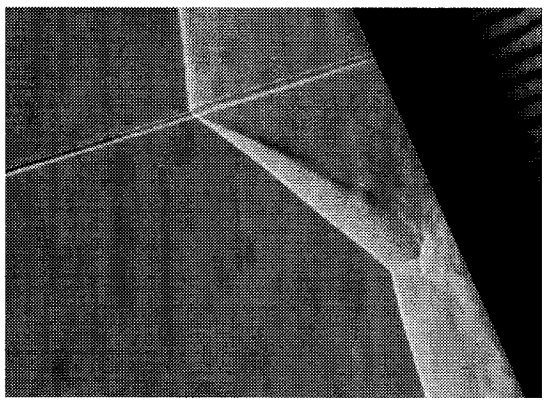

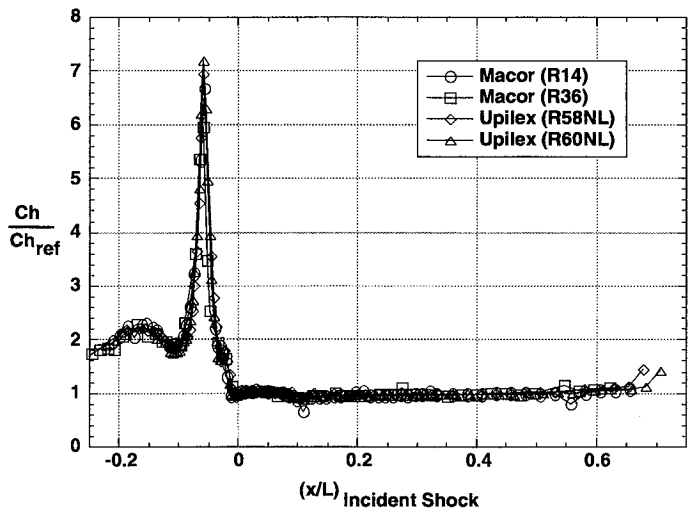


(a) Schlieren image. (b) Heating distribution.

Figure 12: Results for $\lambda = -25°$.

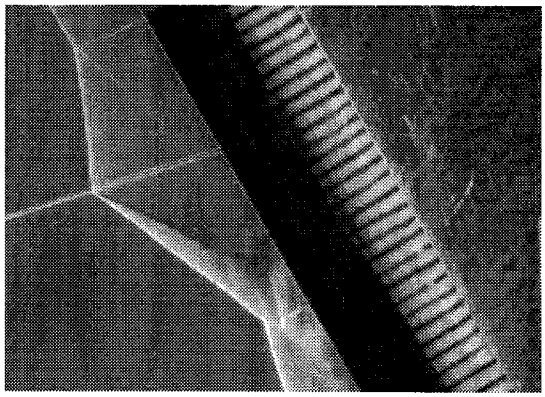

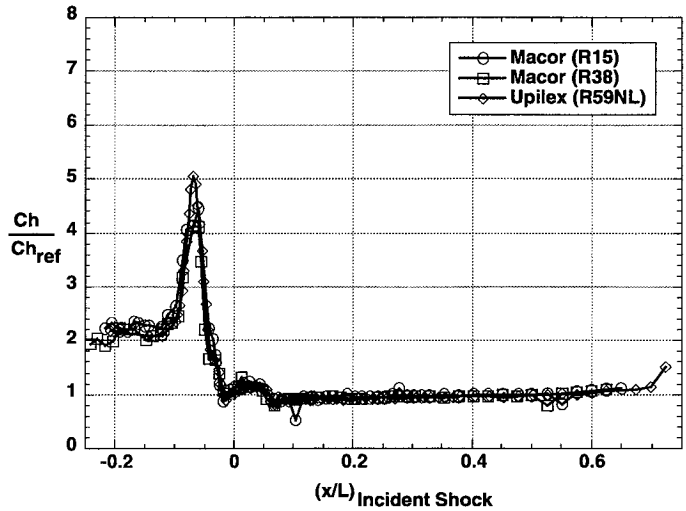


(a) Schlieren image. (b) Heating distribution.

Figure 13: Results for $\lambda = -30°$.

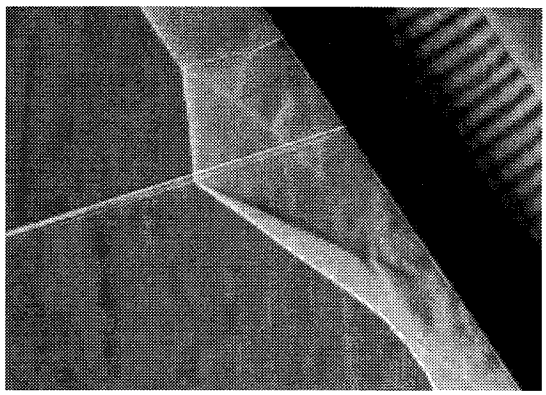

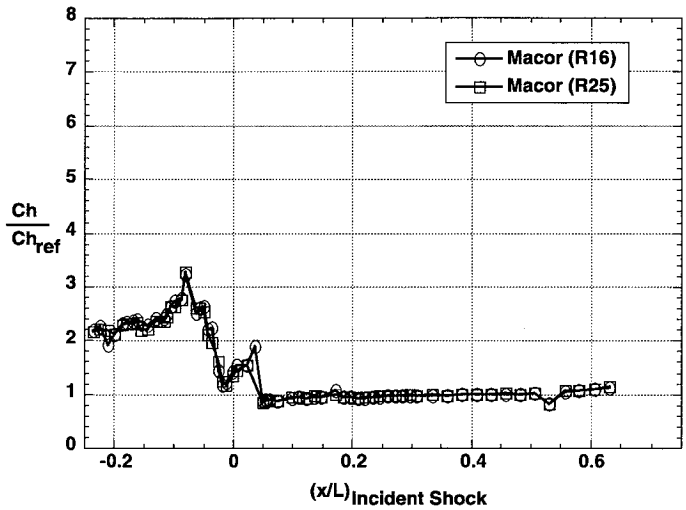


(a) Schlieren image. (b) Heating distribution.

Figure 14: Results for $\lambda = -35°$.

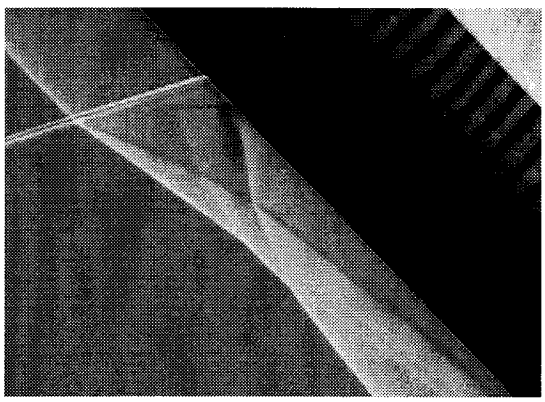

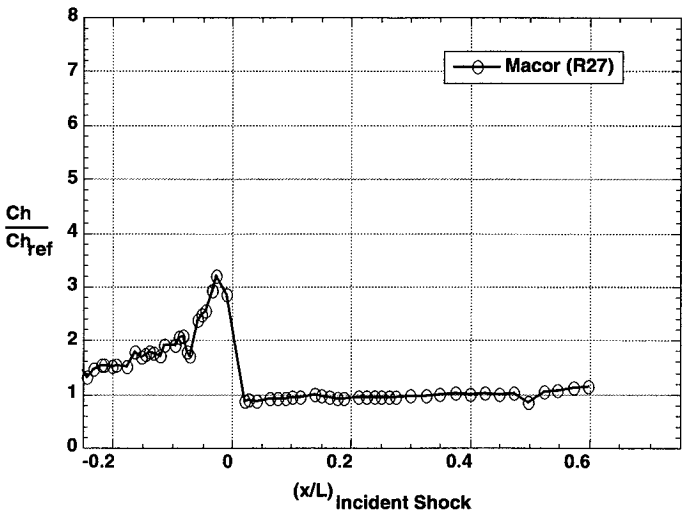


(a) Schlieren image. (b) Heating distribution.

Figure 15: Results for $\lambda = -45°$.

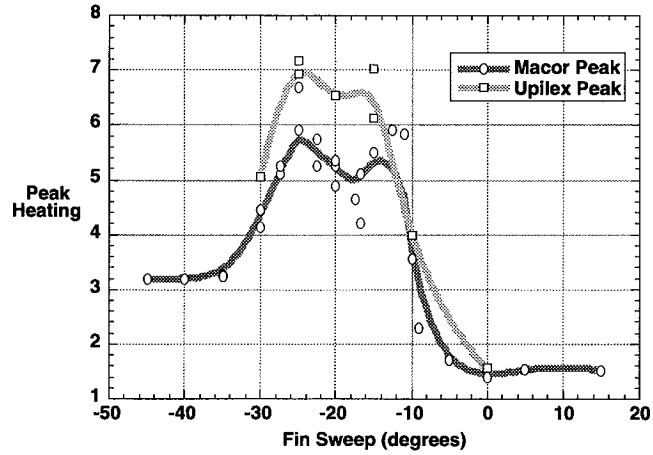


Figure 16: Normalized peak heating values as a function of fin sweep angles.

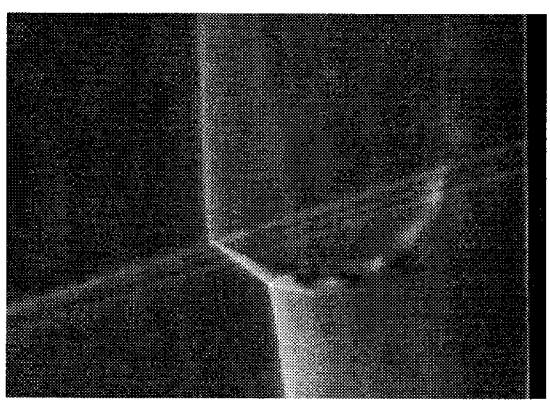

(a) $Re_\infty/ft = 0.5 \times 10^6$.

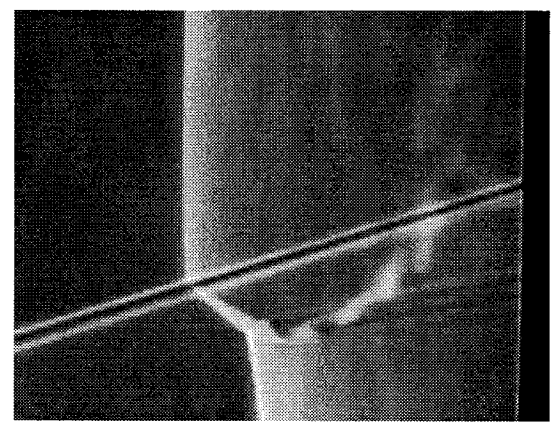

(b) $Re_\infty/ft = 2 \times 10^6$.

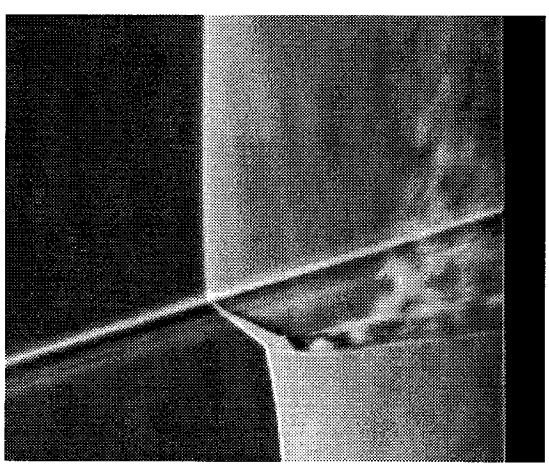

(c) $Re_\infty/ft = 4 \times 10^6$.

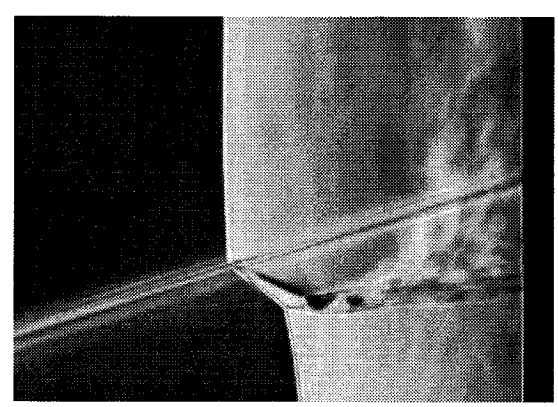

(d) $Re_\infty/ft = 8 \times 10^6$.

Figure 17: Effect of Reynolds number on schlieren image for $\lambda = 0°$

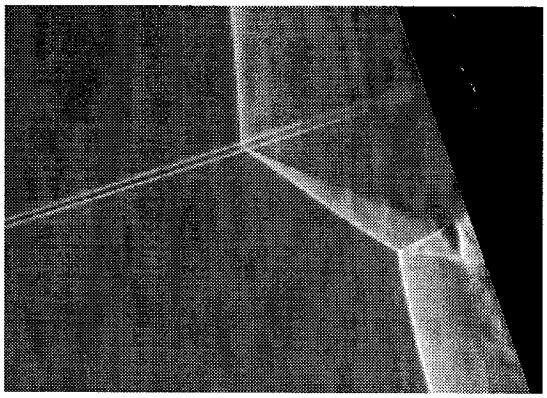

(a) $Re_\infty/ft = 0.5 \times 10^6$.

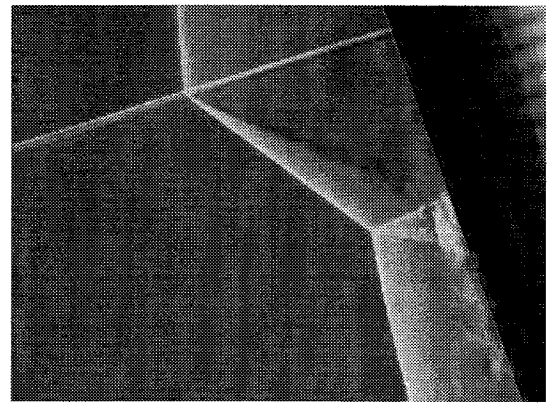

(b) $Re_\infty/ft = 2 \times 10^6$.

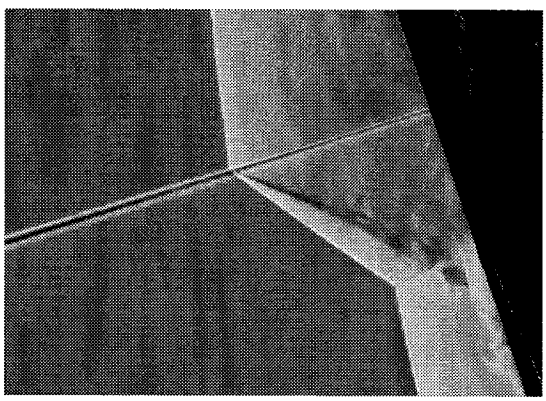

(c) $Re_\infty/ft = 4 \times 10^6$

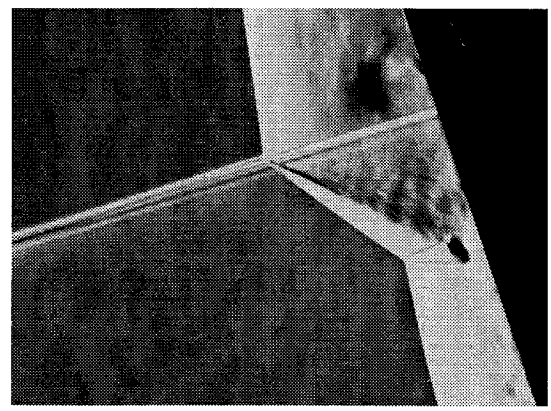

(d) $Re_\infty/ft = 8 \times 10^6$.

Figure 18: Effect of Reynolds number on schlieren for $\lambda = -20°$.

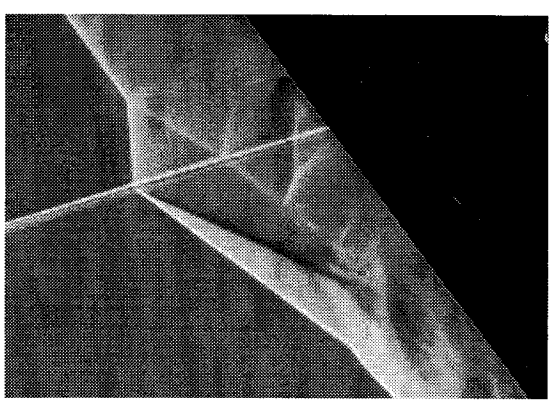

(a) $\lambda = 38°$

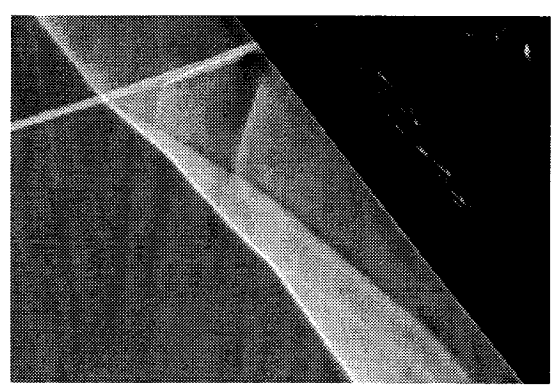

(b) $\lambda = 39°$.

Figure 19: Effect of small fin sweep angle increments at $Re_\infty/ft = 2 \times 10^6$.